Autophagy machinery mediates macroendocytic processing and entotic cell death by targeting single membranes

Oliver Florey[1], **Sung Eun Kim**[1,2], **Cynthia P. Sandoval**[3], **Cole M. Haynes**[1,2], and **Michael Overholtzer**[1,2]

[1]Cell Biology Program, Memorial Sloan Kettering Cancer Center, New York, NY 10065, USA

[2]BCMB Allied Program, Weill Cornell Medical College, 1300 York Avenue, New York, NY 10065, USA

[3]Department of Physiology, University of Arizona, Tucson, AZ 85721, USA

Abstract

Autophagy proteins are normally involved in the formation of double-membrane autophagosomes that mediate bulk cytoplasmic and organelle degradation. Here we report the modification of single-membrane vacuoles in cells by autophagy proteins. Light Chain 3 (LC3), a component of autophagosomes, is recruited to single-membrane entotic vacuoles, macropinosomes, and phagosomes harboring apoptotic cells, in a manner dependent on lipidation machinery including Atg5 and Atg7, and the class III PI-3-kinase Vps34. These downstream components of autophagy machinery, but not the upstream mTor-regulated Ulk- Atg13-Fip200 complex, facilitate lysosome fusion to single membranes and the degradation of internalized cargo. For entosis, a live cell engulfment program, the autophagy protein-dependent fusion of lysosomes to vacuolar membranes leads to the death of internalized cells, which are killed by their hosts. As pathogen-containing phagosomes can be targeted in a similar manner, the death of epithelial cells by this mechanism mimics pathogen destruction. These data define the targeting of single-membrane vacuoles as a property of autophagy pathway proteins in cells in the absence of pathogenic organisms.

Introduction

The proper degradation of material taken into a cell by macroscale endocytic processes[1] is critical for a range of metazoan cell functions including erythroblast enucleation[2], axon pruning[3], removal of dying cells[4], antigen presentation[5], and the clearance of pathogenic organisms[6]. Engulfed cargo is directed toward degradation by a complex series of lipid phosphorylations and protein recruitments that direct phagosome fusion with lysosomes[7]. Critical among these is the recruitment of the lipid kinase Vps34, and accumulation of its product phosphatidylinositol-3-phosphate (PI(3)P), that initiates maturation through stages marked by activation of the small GTPases Rab5 and Rab7, which direct vesicular fusion[8].

Macroautophagy (commonly termed autophagy) is another lysosomal delivery pathway, which mediates formation of double-membrane autophagosomes that enwrap cellular

components for delivery to the lysosome[9]. A signaling complex involving Ulk1, Atg13, and Fip200 is responsible for activating two ubiquitin-like conjugation systems, controlled by autophagy (Atg) proteins (Atg3, 4, 5, 7, 12, 16), that form autophagosomes in part by conjugating Atg8 (Light Chain 3 (LC3)) to phosphatidylethanolamine (PE)[10]. The recovery of amino acids and other building blocks by autophagy is widely viewed as a survival mechanism for cells undergoing starvation[11–13]. The autophagy pathway also targets a variety of pathogenic organisms for degradation by sequestration into double-membrane autophagosomes, including *Listeria monocytogenes*[14, 15], *Mycobacterium tuberculosis*[16], *Streptococcus pyogenes*[17], *Shigella*[18], and *Toxoplasma gondii*[19]. But for *Escherichia coli* and *Saccharomyces cerevisiae*, autophagy pathway proteins have been shown to facilitate killing and degradation by directly conjugating LC3 to phagosome membranes, in a manner independent of double-membrane autophagosomes, suggesting a non-canonical role for autophagy proteins in innate immunity, referred to as LC3-associated phagocytosis or LAP[20 21].

Recently a cell death mechanism was reported called entosis[22]. Entosis, like phagocytosis, is a form of cell engulfment. But unlike phagocytosis that targets dead or dying cells, entosis occurs between live epithelial cells. Internalizing cells play an active role in engulfment, which results in complete internalization within an "entotic vacuole", whose membrane is derived from invagination of the host cell plasma membrane. The cell-in-cell structures resulting from entosis are found in human cancers, but their role remains unknown[23]. Although some entotic cells can escape from their hosts, most undergo cell death, suggesting that entosis could be a mechanism of tumor suppression[22]. While entotic cell death is non-apoptotic and involves lysosomal acidification of the entotic vacuole, the molecular mechanism is not defined.

Here we report the mechanism of cell death by entosis. We find that entotic vacuole membranes surrounding internalized cells recruit the autophagy protein Light Chain 3 (LC3), dependent on autophagy machinery including Atg5, Atg7, and Vps34, but independent of autophagosome formation. LC3-targeted entotic vacuoles recruit lysosomes, resulting in the degradation of internalized cells, which are murdered by their hosts. These data define a mammalian cell death program that shares characteristics with pathogen destruction[21], and that requires autophagy proteins. Remarkably, we also find that apoptotic cell phagosomes in macrophages, and macropinosomes, are targeted by LC3, dependent on autophagy proteins, but independent of autophagosomes. These data demonstrate that the targeting of single-membrane vacuoles is a general function of autophagy pathway proteins that is not restricted to the innate immune system.

Results

LC3 is recruited to single-membrane entotic vacuoles in an autophagosome-independent manner

During entosis, viable cells are internalized inside of host cells for extended periods - from one to many hours - before the majority undergo a non-apoptotic form of cell death[22]. As the autophagy pathway may contribute to cell death in some contexts, we examined autophagy during entotic death by time-lapse imaging the autophagosome marker GFP-LC3. Surprisingly, we discovered a rapid and transient recruitment of GFP-LC3 from host cells onto entotic vacuole membranes (Fig. 1a, Supplementary Information Movie S1, Supplementary Information Fig. S1a)[22]. Lipidation of LC3 to PE was required for recruitment, as GFP-LC3-G120A, a mutant incapable of lipidation, did not recruit to the entotic membrane, whereas mCherry-LC3 imaged in the same cell did recruit (Fig. 1b).

To examine if LC3 was recruited by autophagosome fusion, we imaged live cells by 4D confocal microscopy. Strikingly, increased GFP-LC3 intensity at vacuole membranes was mirrored by a loss of cytoplasmic fluorescence in host cells (Fig. 1c, Supplementary Information Movie S2), but not by a change in the number of GFP-LC3 puncta (Supplementary Information Fig. S1b). We did not observe overt movement of GFP-LC3 puncta to entotic vacuoles, which might be expected if LC3 recruited by autophagosome fusion. Next we examined the GFP-LC3-loaded entotic vacuole by correlative video-light electron microscopy to interrogate its structure. A cell-in-cell structure was imaged by time-lapse microscopy and fixed after the earliest observable recruitment of GFP-LC3 (Fig. 1d). Examination of the same cells by transmission electron microscopy (TEM) revealed a single-membrane structure of the GFP-LC3-loaded entotic vacuole. There were no observable autophagosome contents within the vacuole lumen, which would be expected upon fusion of double-membrane autophagosomes (Fig. 1d, Supplementary Information Fig. S1c, Supplementary Information Movie S3). These data are consistent with a model whereby GFP-LC3 is directly recruited from the cytosolic pool to the single-membrane entotic vacuole, where it is lipidated.

To explore the requirement of autophagy machinery for LC3 recruitment, siRNAs targeting expression of autophagy proteins, as well as the Vps34 inhibitor 3-methyladenine (3-MA)[24], were introduced into cells. Vps34, Atg5, and Atg7 are required for LC3 lipidation[25–27], whereas Fip200 is a component of the upstream Atg1/Ulk complex that initiates autophagosome formation[28–30]. The knockdown of Vps34, Atg5 or Atg7 significantly reduced the percentage of entotic vacuoles that recruited LC3, demonstrating a requirement for lipidation machinery and Vps34 (Fig. 1e, Supplementary Information Fig. S2a). By contrast, knockdown of Fip200, which blocked starvation-induced autophagy similarly to knockdown of Atg5 (Supplementary Information Fig. S2d,f,g), had no effect on LC3 recruitment (Fig. 1e). These data distinguish single-membrane targeting from macroautophagy, and support a model whereby LC3 recruitment to entotic membranes occurs independent of autophagosomes.

Lysosome fusion to entotic vacuoles and internalized cell death

To further characterize the maturation of entotic vacuoles, we examined events upstream and downstream of LC3. The Vps34 product PI(3)P recruits FYVE-domain proteins that function upstream of LC3 in autophagy[27, 31, 32]. A fluorescent reporter of PI(3)P, 2xFYVE-mCherry, recruited to entotic vacuoles, approximately 12 minutes (11.9 mins +/− 4.3) prior to LC3 (Fig. 1f, Supplementary Information Movie S4), suggesting that PI(3)P production at the vacuole membrane could direct LC3 lipidation. We also imaged cells expressing the lysosome marker Lamp1-GFP in combination with mCherry-LC3. Lamp1-GFP recruited to entotic vacuoles approximately 30 minutes after LC3, but still prior to the death of internalized cells (Fig. 1g, Supplementary Information Movie S5). By expressing mCherry-tagged Cathepsin B we also confirmed that lysosomal enzymes from the host cell deposit into the entotic vacuole prior to internalized cell death (Fig. 1h). The recruitment of LC3 and conversion of entotic vacuoles to lysosome compartments prior to cell death suggests that entotic cells are killed by their hosts (Fig 1i,j).

Autophagy lipidation machinery and Vps34 are required for LC3 recruitment and non-apoptotic "killing" of internalized cells

We next examined if LC3 recruitment is required for internalized cell death. By quantifying cell fate following knockdown of Vps34, Atg5 or Atg7, we found a small but significant reduction in internalized cell death (Fig. 2b, Supplementary Information Fig. S2b). By contrast, depletion of Fip200, which had no effect on LC3 recruitment (Fig. 1e), also had no effect on cell fate (Fig. 2b). To localize the requirement of autophagy machinery, cell fates

were quantified in mixed cell-in-cell structures, with Atg5 inhibited in either internalized cells or hosts. Knockdown of Atg5 in hosts but not internalized cells inhibited LC3 recruitment and partially rescued internalized cells from death (Fig. 2c,d), demonstrating that autophagy lipidation machinery in host cells is required for LC3 recruitment and internalized cell killing.

Internalized cells require macroautophagy to survive within entotic vacuoles

Overall, inhibition of internalized cell death by knockdown of autophagy machinery (Fig. 2b) was modest, considering the more than 3-fold inhibition of LC3 recruitment by depleting Atg5 or Atg7 (Fig. 1e). By monitoring cell death morphology with the nuclear marker H2B-mCherry, it was evident that autophagy-inhibited internalized cells were undergoing apoptosis, whereas control cells died non-apoptotically (Fig. 2e). Importantly, knockdown of either Fip200 or Atg5 significantly increased the frequency of apoptosis, linking this phenotype to macroautophagy inhibition. This is reminiscent of previous results where lysosome inhibition switched entotic cell death from non-apoptotic to apoptotic[22]. We hypothesized that internalized cells undergo starvation inside of host cell vacuoles, and rely on autophagy for survival. Internalized cells were restricted for access to growth media, as assessed by uptake of fluorescently-labeled epidermal growth factor (EGF-Alexa488) (Supplementary Information Fig. S3a), and they displayed low levels of phosphorylated S6 ribosomal protein, similar to starved cells (Supplementary Information Fig. S3b).

To determine if internalized cells upregulate autophagy, we quantified red/green fluorescence ratios of cells expressing a tandem-tagged LC3 (GFP-mCherry), which allows for quantification of autophagy due to loss GFP but retention of mCherry fluorescence in lysosomes[33]. Control cells starved in HBSS exhibited increased red/green ratios, consistent with the activation of autophagy, which was inhibited by Vps34 siRNA. Similarly, internalized cells displayed increased red/green ratios, which were inhibited by Vps34, Atg5 or Fip200 knockdown (Fig. 2f). Internalized cells also displayed increased numbers of autophagosomes and autolysosomes identified by TEM (Fig. 2g,h). Together these data demonstrate that internalized cells are denied access to growth media and upregulate macroautophagy as a survival response. Upon macroautophagy inhibition, by siRNA-mediated knockdown of Fip200 or Atg5, internalized cells are sensitized to apoptosis.

Inhibition of autophagy machinery and apoptosis rescues entotic cells and promotes anchorage-independent growth in soft agar

It was previously reported that Bcl2 overexpression inhibited Concanamycin A-induced apoptosis of entotic cells, and the simultaneous inhibition of apoptosis and lysosome function enabled internalized cell release[22]. To achieve a more complete rescue of internalized cells in the context of autophagy protein inhibition, we applied a similar strategy and overexpressed Bcl2 to block apoptosis. The combined inhibition of autophagy proteins and apoptosis reduced internalized cell death more than autophagy protein inhibition alone, and significantly increased the percentage of internalized cells that escaped from their hosts (Fig. 3a).

To examine the potential significance of entotic cell death, we investigated the effects of autophagy protein inhibition on transformed growth in soft agar, where entosis occurs at high frequency[22]. We used non-transformed MCF10A cells, which are competent for apoptosis and entosis, and do not grow under anchorage-independent conditions. The pro-proliferative oncogene HPV-E7, and also Bcl2, were overexpressed in MCF10A cells to activate proliferation and block apoptosis[22]. Despite overexpression of these oncogenes, anchorageindependent growth in soft agar was limited, and entosis occurred at high frequency (~40%, after 48 hours). Entotic structures readily exhibited cell death (Fig. 3c,

Supplementary Information Movie S6), consistent with the ability of entosis to eliminate cells that are resistant to apoptosis[22]. We also found that cells could escape from such structures, even in soft agar (Supplementary Information Movie S6). To examine the role of entosis in this system, we blocked entotic cell death by inhibiting autophagy proteins, or blocked the formation of cell-in-cell structures by inhibiting Rho-kinase with Y27632, as reported[22]. The inhibition of entotic death with 3-MA significantly increased colony formation, and decreased the frequency of cell-in-cell structures in soft agar after 48 hours (Fig 3d,e). Unlike Y27632, which blocks cell-in-cell formation, inhibiting autophagy did not affect the ability of MCF10A cells to form cell-in-cell structures (Fig. 3b), suggesting that the decreased frequency of cell-in-cell in soft agar was due to its effect on reducing cell death, which leads to internalized cell release. Similar to 3-MA, siRNAs targeting *ATG5* also increased colony formation (Fig. 3f,g), demonstrating that autophagy proteins act as negative regulators of transformed growth under these conditions where entosis occurs at high frequency. These data are consistent with entosis, and entotic cell death, acting as a suppressor of transformed growth.

LC3 recruits to apoptotic cell phagosomes

To explore the significance of single-membrane modification by autophagy proteins, we considered whether other, non-pathogen engulfments would also be targeted. We noted that entotic vacuoles were targeted by LC3 even if internalized cells had undergone apoptosis (Fig. 4a,b; Supplementary Information Movie S7). To examine if macrophages ingesting apoptotic cells would recruit LC3 to phagosomes, J774 mouse macrophages expressing GFPLC3 were incubated with apoptotic cells expressing H2B-mCherry. Strikingly, GFP-LC3 was rapidly recruited to apoptotic cell phagosomes, (Fig. 4c, Supplementary Information Movie S8). Following LC3 recruitment, corpses appeared to be degraded rapidly, as evidenced by the release of mCherry from condensed nuclei, which was blocked by treatment with the lysosome inhibitor Concanamycin A (Fig. 4c, Supplementary Information Fig. 4c, Supplementary Movie S8). Correlative light-electron microscopy of the LC3-targeted phagosome revealed a single membrane structure, devoid of fusing vesicles and autophagic bodies as was observed for the entotic vacuole (Fig. 4e), demonstrating that macrophages recruit LC3 to single-membrane apoptotic cell phagosomes. J774 macrophages expressing an shRNA targeting *ATG5*, which inhibited autophagy (Supplementary Information Fig. S4a,b), were significantly inhibited for recruitment of GFP-LC3 to phagosomes (Fig. 4d). Notably, corpses engulfed by shATG5 macrophages resembled those taken in by control macrophages treated with Concanamycin A, as the diffusion of H2B-mCherry, which marks lysosome-mediated degradation, was markedly inhibited (Fig. 4f, Supplementary Information Fig. S5). These data demonstrate a role for autophagy protein targeting of single-membrane phagosomes in regulating the degradation of apoptotic corpses.

Macropinosomes recruit LC3

In J774 macrophages we also noted the recruitment of GFP-LC3 to macropinocytic vacuoles. 50% of macropinosomes rapidly recruited GFP-LC3 (Fig. 5a, Supplementary Information Movie S9) in an ATG5-dependent manner (Fig. 5b). To examine another cell type, we imaged MCF10A, where approximately 50% of macropinosomes also recruited GFP-LC3 (Fig. 5c). Recruitment of GFP-LC3 was inhibited by knockdown of Atg5, but not by the knockdown of Fip200 (Fig. 5d), demonstrating a requirement for autophagy lipidation machinery but independence from macroautophagy. Interestingly, in line with a previous report[21], we found no recruitment of LC3 to phagosomes surrounding uncoated latex beads, while macropinosomes in the same cell did recruit LC3 (Fig. 5e, Supplementary Information Movie S10). Latex bead-containing phagosomes stained positively with Lysotracker, demonstrating their complete engulfment (Fig 5e).

LGG-1 recruits to apoptotic cell phagosomes during *Caenorhabditis elegans* embryo development

To extend our findings to an in vivo model, we examined if LC3 would recruit to apoptotic cell phagosomes during *C. elegans* embryo development[34, 35]. By time-lapse imaging embryos co-expressing mCherry::RAB-5, which is known to recruit to phagosomes[8], and GFP::LGG-1, the LC3 homologue, we indeed observed recruitment of LGG-1 to apoptotic cell phagosomes (Fig. 6a,b; Supplementary Information Fig. S4d, Supplementary Information Movie S11). LGG-1 recruited coincident with, or immediately after, RAB-5 (Fig. 6b). Depletion of the autophagy protein Beclin1 homolog, BEC-1, a component of the Vps34 complex, by RNAi significantly reduced the frequency of both LGG-1 and RAB-5 recruitment (Fig. 6c,d). The knockdown of BEC-1 also increased the number of apoptotic corpses that were observed (Fig. 6e,f), in agreement with a recent report[36]. This did not appear to be due to a defect in apoptotic corpse uptake, but rather a defect in corpse degradation, as corpses from *bec-1* RNAi worms still showed CED-1 recruitment, demonstrating engulfment[37] (Fig. 6g). These data are consistent with a model whereby BEC-1 regulates corpse degradation in *C. elegans*, at least in part by controlling phagosome maturation by the recruitment of RAB-5 and LGG-1.

Discussion

The data presented here demonstrate targeting of single-membrane vacuoles, including entotic vacuoles, apoptotic cell phagosomes, and macropinosomes, by autophagy proteins. Unlike macroautophagy, which is induced by starvation and inactivation of mTor[38], the targeting of single membranes by autophagy proteins occurs in cells under normal growth conditions when mTor is active[39]. Accordingly, single-membrane targeting of LC3 requires lipidation machinery (e.g. Atg5 and Atg7)[25, 26, 40, 41], and Vps34, but does not require Fip200, a member of the mTor-inhibited Ulk complex that is required for macroautophagy[28–30, 42–45].

Efficient degradation of phagocytized *Escherichia coli* or yeast[21], the in vivo resistance to *Toxoplasma gondii*[46] and presentation of exogenous antigen[47], were all recently shown to require autophagy machinery in an autophagosome-independent manner, while relying on the presence of pathogens or Toll-like receptor ligands. We now show a similar role for autophagy proteins in the clearance of apoptotic cells, a process of fundamental importance in the development and homeostasis of multicellular organisms[4]. While autophagy is proposed to play a role in dying cells to expose "eat me" signals[48], our in vitro and in vivo data demonstrate that autophagy proteins also directly regulate the degradation of apoptotic cells by targeting phagosome membranes in engulfing cells. How non-pathogen engulfments promote LC3 targeting remains to be determined, but may relate in part to the mechanism of engulfment; as, interestingly, we found that phagocytosis of an uncoated latex bead does not trigger LC3 recruitment, consistent with previous reports[21, 49], but differing from others[50], while a macropinosome in the same cell does recruit LC3.

Our data suggest a role for autophagy proteins downstream of the Ulk complex, and in particular LC3, in lysosome fusion[51]. Any such roles for LC3 in autophagy would be obscured by the requirement of LC3 and its homologues for autophagosome formation[52, 53]. LC3 has been argued to be dispensable for autophagosome-endosome fusion using an in vitro reconstitution assay[54], but such a role may exist in intact cells. Recently LC3B and the homologous protein Gate-16 were shown to mediate membrane fusion between liposomes[55, 56]. Although fusogenic activity may depend on assay conditions[57], it is conceivable that LC3 mediates membrane fusion between phagosomes and lysosomes directly. Alternatively, one of the host of recently identified LC3-interacting proteins could function in lysosome fusion and require LC3 for targeting[58].

Roles for entosis in tumor promotion, through the generation of aneuploidy[59], and suppression, based on the elimination of matrix-detached cells, have been proposed[22]. Matrix detachment is encountered by tumor cells at early stages of tumor formation, and later stages as cells metastasize in the body and are displaced from their niches[22, 60]. One hallmark of tumor cells is the ability to survive and proliferate in the absence of matrix adhesion, for example in soft agar. Our data identify the mechanism by which entosis eliminates matrix deprived cells. Entotic cells are murdered by their hosts, in an autophagy protein-dependent manner. That autophagy protein inhibitors can significantly increase the transformed growth of cells undergoing high rates of entosis, similar to Rho-kinase inhibition, suggests that entosis suppresses transformed growth by inducing cell death, using machinery of the autophagy pathway.

Experimental Procedures

Antibodies and reagents

Anti-LC3B (1:2000) and anti-Tubulin (1:2000) (Sigma), anti-ATG5 (1:1000), anti-ATG7 (1:1000) and anti-phospho Ribosomal Protein S6 (Cell Signaling), anti- GAPDH (1:1000) (SCBT). The following inhibitors and reagents were used at the indicated concentrations, 3-methyladenine (3-MA) (Sigma) 3mM; Y27632 (EMD) 10µM and LysoTracker Red DND-99 (Invitrogen) 50nM.

Constructs

pBabe-GFP-LC3, pBabe-mCherry-LC3, pMLP-IRES-shATG5 and 2XFYVEm-Cherry (FYVE domain from Hrs) were a kind gift from Dr. X. Jiang, MSKCC. Tandem pBabe-GFP-mCherry-LC3 was a kind gift from Dr. J. Debnath, UCSF. pRetro-LAMP1-GFP was cloned by inserting the rat LAMP1 sequence (from addgene plasmid#1817) into the BamHI-EcoRI sites of the pRetroQ-AcGFP1-N1 vector (Clontech). pBabe-CathepsinB-mCherry was cloned by inserting CathepsinB-mCherry into the BamHI-SalI sites of pBabepuro. The pBabepuro-Bcl2, and pLXSN-HPV-E7 constructs were a kind gift of Dr. J.S. Brugge, Harvard Medical School, and have been described elsewhere[61]. The pBabe-H2B-mCherry and pBabe-mCherry-CAAX constructs were gifts of Dr. C. Leong and Dr. J.S. Brugge, Harvard Medical School.

Virus production and infection

For virus infection, cells were seeded in a 6 well plate at 5×10^4 per well. The next day 1ml viral supernatant was added with 10µg/ml polybrene for 24 hours followed by a media change. Cells were then selected with the appropriate antibiotic, puromycin (2µg/ml), G418 (200µg/ml), or blasticidin (10µg/ml).

siRNA

siGenome SMART pool siRNAs and individual oligos against human *VPS34*, *ATG5*, *ATG7* and *FIP200* were obtained from Dharmacon, Chicago, IL. MCF10A cells were seeded in a 6 well plate at 6×10^4 per well and transfected with 100nM siRNA using Oligofectamine (Invitrogen). Cells were routinely assayed 48 hours post transfection.

Tissue Culture

MCF10A cells were cultured as previously described[62] in DME/F12 + 5% horse serum, 20 ng/ml EGF, 10 µg/ml insulin or 100 ng/ml IGF-I, 0.5 µg/ml hydrocortisone, 100 ng/ml cholera toxin, 50 U/ml penicillin, and pen/strep. MCF10A cells overexpressing E7 and Bcl2 were generated as described[61]. MCF7 cells were obtained from the Lombardi Cancer Center at Georgetown University, J774 mouse macrophages (ATCC) and HEK293 cells (ATCC)

were cultured in DMEM + 10% FBS with pen/strep. U937 human monocytic cells were cultured in RPMI-1640 + 10% FBS with pen/strep.

Microscopy

To quantify entotic cell fate, 1.5×10^5 cells were seeded overnight on 35mm glass-bottomed dishes (MatTek, Ashland, MA) and cell-in-cell structures were imaged by time-lapse microscopy the next day. Fluorescence and differential interference contrast (DIC) images were acquired every 4 minutes for 20 hours using a Nikon Ti-E inverted microscope attached to a CoolSNAP CCD camera (Photometrics), and NIS Elements software (Nikon). Only live internalized cells at the start of time-lapse were quantified for cell fate. Internalized cells were scored for release, death or no change. Control experiments demonstrated that >95% of cell-in-cell structures chosen for analysis were completely enclosed and shielded from external media at the start of imaging, as assessed by FM4-64 staining. Entotic structures chosen by DIC were stained with FM4-64, which labels membranes in contact with external media. The numbers of structures staining positive or negative were quantified (Supplementary Fig. 3c). The timing and type of internalized cell death was determined by DIC morphology, cessation of movement or, where present, monitoring nuclear markers. Inhibitors were added, as indicated, 30 minutes prior to image acquisition. For mixed cultures, H2B-mCherry expressing cells were plated with GFP-LC3 expressing cells at a 1:1 ratio. Confocal imaging was performed with the Ultraview Vox spinning disc confocal system (Perkin Elmer) equipped with a Yokogawa CSU-X1 spinning disc head, and EMCCD camera (Hamamatsu C9100-13), and coupled with a Nikon Ti-E microscope. All imaging with live cells was performed within incubation chambers at 37°C and 5% CO_2. Confocal image acquisition and analysis was performed with Volocity software (Perkin Elmer).

Electron microscopy

Cells were grown on grid etched Aclar film, and imaged by fluorescence microscopy until LC3 recruitment to vacuole membranes. Samples were then fixed in 2.5% Glutaraldehyde / 2% Paraformaldehyde in 0.075M Cacodylate buffer pH 7.5 for one hour followed by rinsing in Cacoldylate buffer and post fixation in 2% Osmium Tetroxide for one hour. The samples were then rinsed in double distilled water followed by dehydration in a graded series of alcohol 50%, 75% 95% through absolute alcohol and overnight in 1: 1 Proplene Oxide / Poly Bed 812. The samples were then embedded the following day, onto Poly Bed 812 filled Beem capsules and cured in an oven at 60°C for two days. Following immersion in liquid nitrogen, Aclar film was then ripped from the capsules and ultra thin sections were obtained with a Reichert Ulltracut S microtome. Sections were stained with Uranyl Acetate and Lead Citrate. Images were obtained using a JEOL 1200 EX Transmission Electron microscope.

Measuring autophagy using tandem GFP-mCherry-LC3

MCF10A cells expressing GFP-mCherry-LC3 were plated on glass-bottom coverslip dishes. Internalized entotic cells, or control single cells, +/− HBSS (12 hours), were imaged by confocal microscopy in the presence or absence of *VPS34, ATG5* or *FIP200* siRNA. Fluorescence intensities of mCherry and GFP were measured in cells using Volocity software. Data were normalized against background and mCherry/GFP ratios calculated.

Measuring autophagy by electron microscopy

MCF10A cells were seeded on non-adherent plates for 6 hours to induce a high frequency of cell-in-cell formation. Cells were then seeded onto glass coverslips overnight. Following this, cells were trypsinized, pelleted and fixed in 2.5% Glutaraldehyde / 2% Paraformaldehyde in 0.075M Cacodylate buffer pH 7.5 for one hour. Pellets were then

processed as above. 3 or more fields of view were acquired within the cytoplasm of internalized or single cells, 10 individual cells were used in each group. The area of autophagosomes and autolysosomes was calculated as a percentage of cytoplasm using ImageJ software (NIH).

Apoptotic phagocytosis, latex bead, and macropinosome assays

For apoptotic phagocytosis assays, J774 cells were seeded onto glass-bottom coverslip dishes in the presence of 200U/ml IFNγ for 2 days. U937 cells expressing H2B-mCherry were stimulated with $80J/m^2$ to induce apoptosis and added to J774 cultures at 4×10^6 per dish. Where indicated, 100nM Concanamycin A was added before image acquisition. For latex beads (Polysciences, Inc, PA), 3µm beads were added to macrophage at a ratio of 10:1. Cells were monitored for 20 hours, and z-stacks were acquired every 10 minutes. For MCF10A macropinosome assays, 10kD red fluorescent dextran was added to culture media (0.1mg/ml) for 10min, followed by washing in media for 5min, and confocal imaging (0.5µm z-stacks) of red dextran-labeled macropinosomes at 1min intervals for 30min to monitor recruitment of GFP-LC3. For J774 macropinosome assays, cells were imaged by confocal microscopy in the presence of 10kD red dextran (0.1mg/ml). Lysotracker red (Invitrogen) was added to cultures (50nm) after the timelapse imaging to image acidification of phagosomes.

Imaging *C.elegans* apoptotic phagocytosis

The mCherry::RAB-5; GFP::LGG-1 expressing strain was generated by crossing the *pie-1$_{pr}$::mCherry::rab-5* allele from strain RT1043 into the *lgg-1$_{pr}$::lgg-1::gfp* expressing strain (DA2123). Both strains were provided by the *Caenorhabditis* Genetics Center (University of Minnesota, Minneapolis, MN). RNAi experiments were performed by bacterial feeding as described previously[63]. Embryos obtained from dissected gravid hermaphrodites were placed on 2% agarose pads and mounted on a coverslip for observation using an Ultraview Vox spinning disc confocal system (Perkin Elmer) equipped with a Yokogawa CSU-X1 spinning disc head, and EMCCD camera (Hamamatsu C9100-13), and coupled with a Nikon Ti-E microscope. For apoptotic corpse counting, embryos at different developmental stages, as assessed by morphology, were imaged by DIC. Corpses were identified by morphology and counted.

Western blotting

Cells were scraped into ice-cold RIPA buffer (50mM Tris pH 7.4, 150mM NaCl, 2mM EDTA, 1% NP40, 0.1% SDS + protease inhibitor cocktail) and lysed for 10 minutes on ice. Lysates were centrifuged 13,000rpm at 4°C for 12 minutes and protein quantified by BCA assay (Pierce, Rockford, IL). Samples were separated on 10% polyacrylamide SDS-PAGE gels (15% for LC3 blots), and transferred to a polyvinyldifluoride membrane. The membrane was blocked into TBS-T + 5% BSA and incubated overnight at 4°C with primary antibodies diluted blocking buffer. Blots were incubated with horseradish peroxidase conjugated to secondary antibodies and protein detected using enhanced chemiluminescence (Invitrogen). Densitometry analysis was carried out using ImageJ software (NIH).

Quantitative PCR

Total RNA was prepared using the RNAeasy mini kit (Qiagen) 48 hours after transfection of cells with siRNA. Quantitative PCR was performed using the Bio-Rad iCycler real-time system (MyiQ), with SYBR green detection (iScript One-Step RT-PCR Kit with SYBR green (Bio-Rad)). Samples were analyzed by the standard curve method in triplicate. Reactions contained a single product as determined by agarose gel electrophoresis and melting curve analysis. The following primer pairs were used: *ACTIN* For

AGAGCTACGAGCTGCCTGAC ; *ACTIN* Rev AGCACTGTGTTGGCGTACAG; *FIP200* For GTGCTGGGACGGATACAAAT; *FIP200* Rev TTTCCAATGCAAGCTGTGTC.

Cell-in-cell formation – suspension assay

MCF10A (1×10^5 cells) pretreated with Vps34 or ATG5 siRNA, or in the presence of 3-MA or Y27632 were plated in non-adherent 6-well dishes for 7 hours. Cytospins of cells were made and stained for E-cadherin and β-catenin. The percentage of cells in cell-in-cell structures was quantified by counting >300 cells per slide.

Colony formation in soft agar

5×10^4 MCF10A cells overexpressing E7 and Bcl2 were added to 1ml of growth medium with 0.3% agar and layered onto 1ml of 0.5% agar beds in six-well plates and covered in 1ml liquid growth media. Cells were fed with 1ml of liquid medium every 5 days for 2 weeks, after which colonies were stained with 0.02% iodonitrotetrazolium chloride (Sigma–Aldrich) and quantified using an Optronix Gelcount colony counter (Oxford Optronix Ltd., Oxford, UK). Assays were conducted in duplicate in three independent experiments. Where indicated, 3-MA (3mM) or Y27632 were included in all solutions. Counts of cell-in-cell structures were made by light microscopy, 48 hours after seeding in soft agar.

Statistics

Indicated *P* values were obtained using the Student's t-test, or Chi-square test where indicated.

Supplementary Material

Refer to Web version on PubMed Central for supplementary material.

Acknowledgments

References

1. Kumari S, Mg S, Mayor S. Endocytosis unplugged: multiple ways to enter the cell. Cell Res. 2010; 20:256–275. [PubMed: 20125123]

2. Kawane K, et al. Requirement of DNase II for definitive erythropoiesis in the mouse fetal liver. Science. 2001; 292:1546–1549. [PubMed: 11375492]

3. Broadie K. Axon pruning: an active role for glial cells. Curr Biol. 2004; 14:R302–R304. [PubMed: 15084298]

4. Elliott MR, Ravichandran KS. Clearance of apoptotic cells: implications in health and disease. J Cell Biol. 2010; 189:1059–1070. [PubMed: 20584912]

5. Savina A, Amigorena S. Phagocytosis and antigen presentation in dendritic cells. Immunol Rev. 2007; 219:143–156. [PubMed: 17850487]

6. Haas A. The phagosome: compartment with a license to kill. Traffic. 2007; 8:311–330. [PubMed: 17274798]

7. Steinberg BE, Grinstein S. Pathogen destruction versus intracellular survival: the role of lipids as phagosomal fate determinants. J Clin Invest. 2008; 118:2002–2011. [PubMed: 18523652]

8. Kinchen JM, et al. A pathway for phagosome maturation during engulfment of apoptotic cells. Nat Cell Biol. 2008; 10:556–566. [PubMed: 18425118]

9. Yang Z, Klionsky DJ. Eaten alive: a history of macroautophagy. Nat Cell Biol. 2010; 12:814–822. [PubMed: 20811353]

10. Yang Z, Klionsky DJ. Mammalian autophagy: core molecular machinery and signaling regulation. Curr Opin Cell Biol. 2010; 22:124–131. [PubMed: 20034776]

11. Jin S, White E. Tumor suppression by autophagy through the management of metabolic stress. Autophagy. 2008; 4:563–566. [PubMed: 18326941]

12. Burman C, Ktistakis NT. Autophagosome formation in mammalian cells. Semin Immunopathol. 2010

13. Levine B, Yuan J. Autophagy in cell death: an innocent convict? J Clin Invest. 2005; 115:2679–2688. [PubMed: 16200202]

14. Rich KA, Burkett C, Webster P. Cytoplasmic bacteria can be targets for autophagy. Cell Microbiol. 2003; 5:455–468. [PubMed: 12814436]

15. Yano T, et al. Autophagic control of listeria through intracellular innate immune recognition in drosophila. Nat Immunol. 2008; 9:908–916. [PubMed: 18604211]

16. Gutierrez MG, et al. Autophagy is a defense mechanism inhibiting BCG and Mycobacterium tuberculosis survival in infected macrophages. Cell. 2004; 119:753–766. [PubMed: 15607973]

17. Nakagawa I, et al. Autophagy defends cells against invading group A Streptococcus. Science. 2004; 306:1037–1040. [PubMed: 15528445]

18. Ogawa M, et al. Escape of intracellular Shigella from autophagy. Science. 2005; 307:727–731. [PubMed: 15576571]

19. Ling YM, et al. Vacuolar and plasma membrane stripping and autophagic elimination of Toxoplasma gondii in primed effector macrophages. J Exp Med. 2006; 203:2063–2071. [PubMed: 16940170]

20. Sanjuan MA, Milasta S, Green DR. Toll-like receptor signaling in the lysosomal pathways. Immunol Rev. 2009; 227:203–220. [PubMed: 19120486]

21. Sanjuan MA, et al. Toll-like receptor signalling in macrophages links the autophagy pathway to phagocytosis. Nature. 2007; 450:1253–1257. [PubMed: 18097414]

22. Overholtzer M, et al. A nonapoptotic cell death process, entosis, that occurs by cell-in-cell invasion. Cell. 2007; 131:966–979. [PubMed: 18045538]

23. Overholtzer M, Brugge JS. The cell biology of cell-in-cell structures. Nat Rev Mol Cell Biol. 2008; 9:796–809. [PubMed: 18784728]

24. Seglen PO, Gordon PB. 3-Methyladenine: specific inhibitor of autophagic/lysosomal protein degradation in isolated rat hepatocytes. Proc Natl Acad Sci U S A. 1982; 79:1889–1892. [PubMed: 6952238]

25. Ichimura Y, et al. A ubiquitin-like system mediates protein lipidation. Nature. 2000; 408:488–492. [PubMed: 11100732]

26. Hanada T, et al. The Atg12-Atg5 conjugate has a novel E3-like activity for protein lipidation in autophagy. J Biol Chem. 2007; 282:37298–37302. [PubMed: 17986448]

27. Petiot A, Ogier-Denis E, Blommaart EF, Meijer AJ, Codogno P. Distinct classes of phosphatidylinositol 3'-kinases are involved in signaling pathways that control macroautophagy in HT-29 cells. J Biol Chem. 2000; 275:992–998. [PubMed: 10625637]

28. Jung CH, et al. ULK-Atg13-FIP200 complexes mediate mTOR signaling to the autophagy machinery. Mol Biol Cell. 2009; 20:1992–2003. [PubMed: 19225151]

29. Hosokawa N, et al. Nutrient-dependent mTORC1 association with the ULK1-Atg13-FIP200 complex required for autophagy. Mol Biol Cell. 2009; 20:1981–1991. [PubMed: 19211835]

30. Ganley IG, et al. ULK1.ATG13.FIP200 complex mediates mTOR signaling and is essential for autophagy. J Biol Chem. 2009; 284:12297–12305. [PubMed: 19258318]

31. Stenmark H, Aasland R, Toh BH, D'Arrigo A. Endosomal localization of the autoantigen EEA1 is mediated by a zinc-binding FYVE finger. J Biol Chem. 1996; 271:24048–24054. [PubMed: 8798641]

32. Eskelinen EL, et al. Inhibition of autophagy in mitotic animal cells. Traffic. 2002; 3:878–893. [PubMed: 12453151]

33. Kimura S, Noda T, Yoshimori T. Dissection of the autophagosome maturation process by a novel reporter protein, tandem fluorescent-tagged LC3. Autophagy. 2007; 3:452–460. [PubMed: 17534139]

34. Sulston JE, Horvitz HR. Post-embryonic cell lineages of the nematode, Caenorhabditis elegans. Dev Biol. 1977; 56:110–156. [PubMed: 838129]

35. Sulston JE, Schierenberg E, White JG, Thomson JN. The embryonic cell lineage of the nematode Caenorhabditis elegans. Dev Biol. 1983; 100:64–119. [PubMed: 6684600]

36. Ruck A, et al. The Atg6/Vps30/Beclin1 ortholog BEC-1 mediates endocytic retrograde transport in addition to autophagy in C. elegans. Autophagy. 7

37. Zhou Z, Hartwieg E, Horvitz HR. CED-1 is a transmembrane receptor that mediates cell corpse engulfment in C. elegans. Cell. 2001; 104:43–56. [PubMed: 11163239]

38. Kamada Y, Sekito T, Ohsumi Y. Autophagy in yeast: a TOR-mediated response to nutrient starvation. Curr Top Microbiol Immunol. 2004; 279:73–84. [PubMed: 14560952]

39. Kim DH, et al. mTOR interacts with raptor to form a nutrient-sensitive complex that signals to the cell growth machinery. Cell. 2002; 110:163–175. [PubMed: 12150925]

40. Mizushima N, et al. A protein conjugation system essential for autophagy. Nature. 1998; 395:395–398. [PubMed: 9759731]

41. Mizushima N, Sugita H, Yoshimori T, Ohsumi Y. A new protein conjugation system in human. The counterpart of the yeast Apg12p conjugation system essential for autophagy. J Biol Chem. 1998; 273:33889–33892. [PubMed: 9852036]

42. Hara T, et al. FIP200, a ULK-interacting protein, is required for autophagosome formation in mammalian cells. J Cell Biol. 2008; 181:497–510. [PubMed: 18443221]

43. Cheong H, et al. Atg17 regulates the magnitude of the autophagic response. Mol Biol Cell. 2005; 16:3438–3453. [PubMed: 15901835]

44. Kabeya Y, et al. Atg17 functions in cooperation with Atg1 and Atg13 in yeast autophagy. Mol Biol Cell. 2005; 16:2544–2553. [PubMed: 15743910]

45. Kamada Y, et al. Tor-mediated induction of autophagy via an Apg1 protein kinase complex. J Cell Biol. 2000; 150:1507–1513. [PubMed: 10995454]

46. Zhao Z, et al. Autophagosome-independent essential function for the autophagy protein Atg5 in cellular immunity to intracellular pathogens. Cell Host Microbe. 2008; 4:458–469. [PubMed: 18996346]

47. Lee HK, et al. In vivo requirement for Atg5 in antigen presentation by dendritic cells. Immunity. 2010; 32:227–239. [PubMed: 20171125]

48. Qu X, et al. Autophagy gene-dependent clearance of apoptotic cells during embryonic development. Cell. 2007; 128:931–946. [PubMed: 17350577]

49. Huang J, et al. Activation of antibacterial autophagy by NADPH oxidases. Proc Natl Acad Sci U S A. 2009; 106:6226–6231. [PubMed: 19339495]

50. Shui W, et al. Membrane proteomics of phagosomes suggests a connection to autophagy. Proc Natl Acad Sci U S A. 2008; 105:16952–16957. [PubMed: 18971338]

51. Kabeya Y, et al. LC3, a mammalian homologue of yeast Apg8p, is localized in autophagosome membranes after processing. EMBO J. 2000; 19:5720–5728. [PubMed: 11060023]

52. Weidberg H, et al. LC3 and GATE-16/GABARAP subfamilies are both essential yet act differently in autophagosome biogenesis. EMBO J. 2010; 29:1792–1802. [PubMed: 20418806]

53. Fujita N, et al. An Atg4B mutant hampers the lipidation of LC3 paralogues and causes defects in autophagosome closure. Mol Biol Cell. 2008; 19:4651–4659. [PubMed: 18768752]

54. Morvan J, et al. In vitro reconstitution of fusion between immature autophagosomes and endosomes. Autophagy. 2009; 5:676–689. [PubMed: 19337031]

55. Nakatogawa H, Ichimura Y, Ohsumi Y. Atg8, a ubiquitin-like protein required for autophagosome formation, mediates membrane tethering and hemifusion. Cell. 2007; 130:165–178. [PubMed: 17632063]

56. Weidberg H, et al. LC3 and GATE-16 N termini mediate membrane fusion processes required for autophagosome biogenesis. Dev Cell. 20:444–454. [PubMed: 21497758]

57. Nair U, et al. SNARE Proteins Are Required for Macroautophagy. Cell. 146:290–302. [PubMed: 21784249]

58. Behrends C, Sowa ME, Gygi SP, Harper JW. Network organization of the human autophagy system. Nature. 2010; 466:68–76. [PubMed: 20562859]

59. Krajcovic M, et al. A non-genetic route to aneuploidy in human cancers. Nat Cell Biol. 13:324–330. [PubMed: 21336303]

60. Horbinski C, Mojesky C, Kyprianou N. Live free or die: tales of homeless (cells) in cancer. Am J Pathol. 2010; 177:1044–1052. [PubMed: 20639456]

61. Debnath J, et al. The role of apoptosis in creating and maintaining luminal space within normal and oncogene-expressing mammary acini. Cell. 2002; 111:29–40. [PubMed: 12372298]

62. Debnath J, Muthuswamy SK, Brugge JS. Morphogenesis and oncogenesis of MCF-10A mammary epithelial acini grown in three-dimensional basement membrane cultures. Methods. 2003; 30:256–268. [PubMed: 12798140]

63. Kamath RS, Martinez-Campos M, Zipperlen P, Fraser AG, Ahringer J. Effectiveness of specific RNA-mediated interference through ingested double-stranded RNA in Caenorhabditis elegans. Genome Biol. 2001; 2 RESEARCH0002.
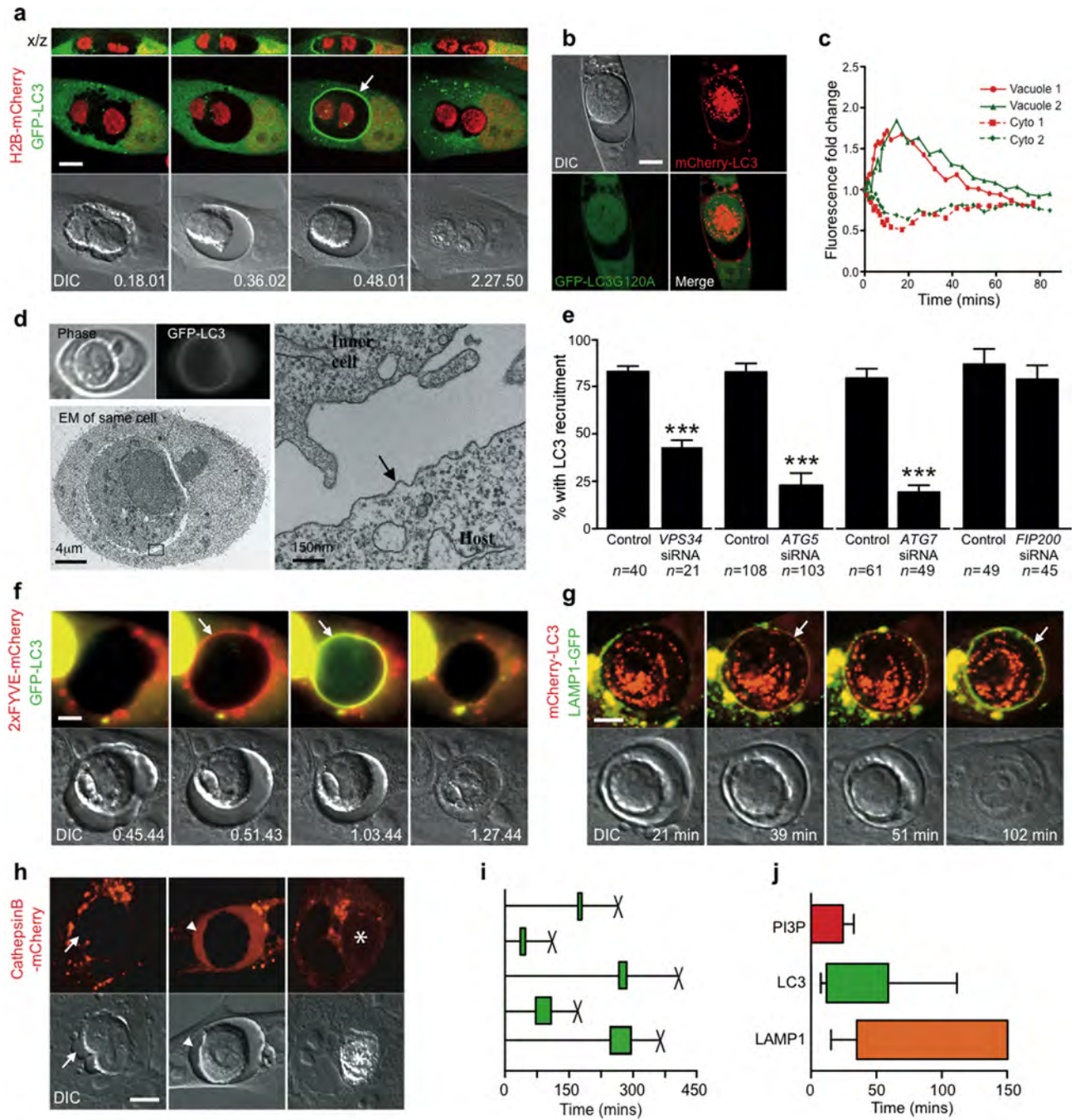
Figure 1.
Entotic cell death involves recruitment of LC3 to a single-membrane vacuole. (a) Confocal time-lapse images of an MCF10A cell-in-cell structure expressing GFP-LC3 and H2B-mCherry. Arrow marks recruitment of LC3 to the entotic vacuole, see Supplementary Information Movie S1. Bar = 15µm. (b) Images of MCF10A expressing GFP-LC3G120A and mCherry-LC3; note no recruitment of GFP-LC3G120A to entotic vacuole. Bar = 15µm (c) LC3 recruits from host cell cytosol onto the entotic vacuole membrane. Data points are mean fluorescence intensity of GFP-LC3 on vacuoles versus cytoplasm for two independent cell-in-cell structures, see Supplementary Information Movie S2. (d) Correlative video-light electron microscopy of MCF10A GFP-LC3 cell-in-cell structure. Cells were imaged by

time-lapse, followed by fixation after LC3 recruitment, see Supplementary Information Movie S3. Post-fixation images (top panels) of phase and GFP were taken demonstrating LC3 recruitment. Electron microscopy of the same cell shows the entotic vacuole is a single membrane (arrow). (e) Percentage of MCF10A cell-in-cell structures, with and without autophagy inhibition, that show LC3 recruitment associated with death of internalized cell. Data represent mean +/− SEM from at least 3 independent experiments, n=total number of death events. *P<0.03, ***P<0.0001. Time-lapse images of MCF10A cell-in-cell structures expressing either: (f) 2xFYVE-mCherry (red) and GFP-LC3 (green), or (g) Lamp1-GFP (green) and mCherry-LC3 (red). Arrows indicate recruitments to the entotic vacuole, see Supplementary Information Movies S4 and S5. Times are indicated as hr:min:sec (f) or min (g). Bar = 5µm. (h) Representative images of cell-in-cell structures where only host cells express CathepsinB-mCherry. Live inner cell with no CathepsinB in the vacuole, arrow (left panel), live internalized cell with CathepsinB from the host inside of the vacuole, arrow head (middle panel), dead internalized cell with CathepsinB from the host throughout the corpse, asterisk (right panel). Bar = 15µm. (i) Five representative timings of GFP-LC3 recruitment to entotic vacuoles (green bar) and death of internalized cells (X) from time-lapse microscopy. (j) Initiation and duration of 2xFYVE domain (red bar, n=11), LC3 (green bar, n=20) and Lamp1 (orange bar, n=7) recruitment to entotic vacuoles, determined using double expressing cells shown in (f, g). Error bars represent SD.
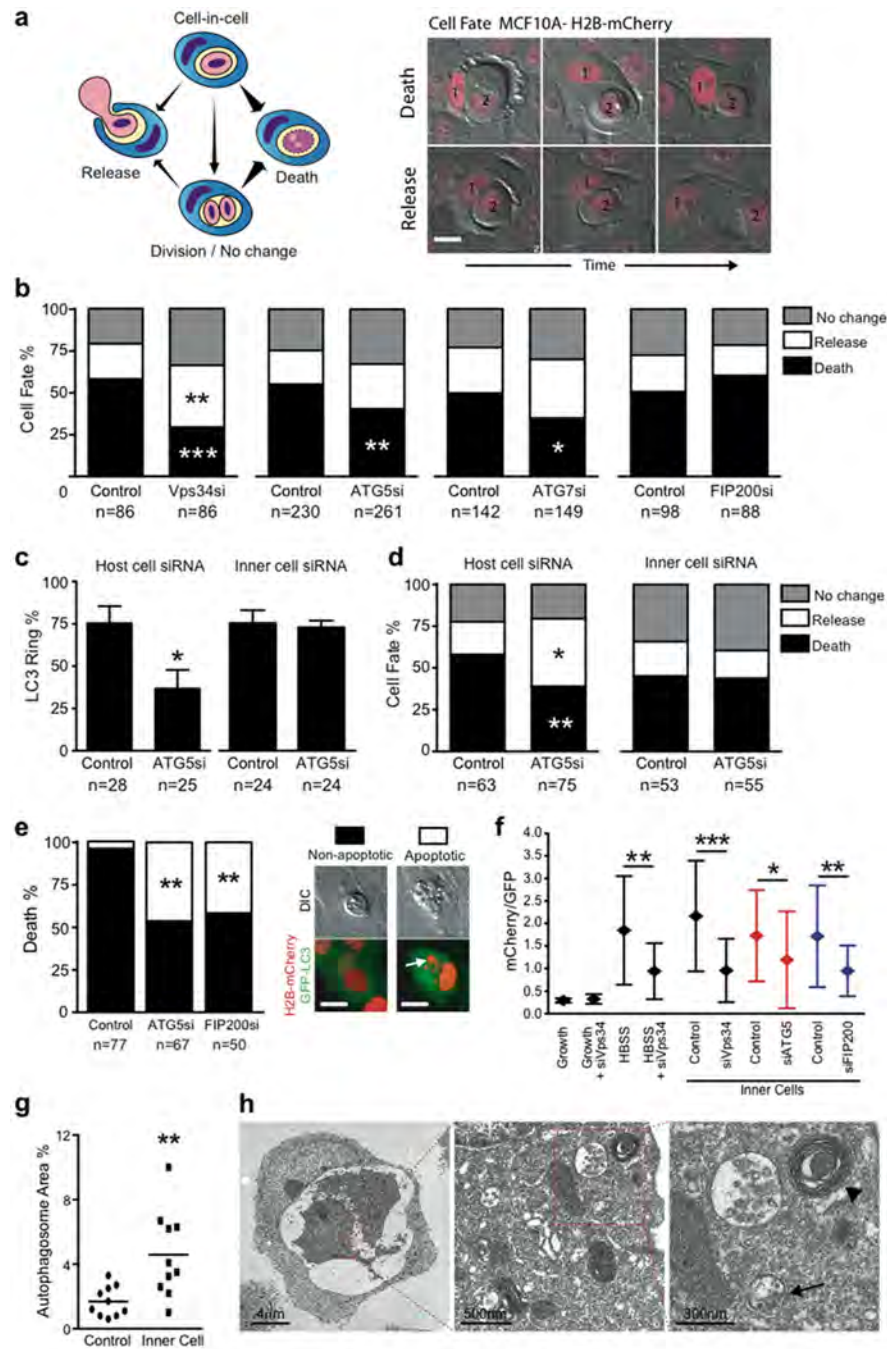
Figure 2.
Autophagy machinery in host cells controls the fate of starving internalized cells. (a) Model depicting the multiple cell fates of internalized cells; arrow thickness represents relative frequency of events. Images of cell-in-cell structures (1=host cell, 2=internalized cell) that show a cell death (top images) or release event (bottom images). Bar = 15µm. (b) Quantification of MCF10A internalized cell fate over 20 hours following autophagy inhibition. Data represent mean from at least 3 independent experiments, n=total number of structures analyzed, #P<0.02, ##P<0.007, *P<0.01, **P<0.004. (c, d) Quantification of LC3 recruitment (c), and cell fate (d), of mixed cell-in-cell structures where host or internalized cells were treated with *ATG5* siRNA. Data represent mean +/− SEM from 3 separate

experiments. *P<0.01, **P<0.004. (e) Quantification of type of internalized cell death after autophagy inhibition, n=total death events analyzed. Data represent mean of 3 independent experiments. **P<0.03. Representative images of non-apoptotic and apoptotic death of internalized cell; arrow points to fragmented apoptotic nuclei. Bar = 15µm. (f) Quantification of mCherry/GFP ratio of live MCF10A single cells or internalized cells expressing tandem GFP-mCherry-LC3, with or without siRNA treatment as indicated. Data represent mean +/− SD; n= numbers of cells analyzed for each data point (from left to right) 30, 30, 30, 25, 30, 25, 25, 25, 30, 27.; *P<0.03, **P<0.003, ***P<0.0004. (g) Quantification of percentage of autophagosome and autolysosome area in control MCF10A (n=10) and internalized cell (n=10) cytoplasm imaged by electron microscopy, **P<0.005. (h) Representative electron micrographs of cell-in-cell structures (left panel), internalized cell cytoplasm (middle and right panel) showing autophagosomes (arrow) and autolysosomes (arrow head).
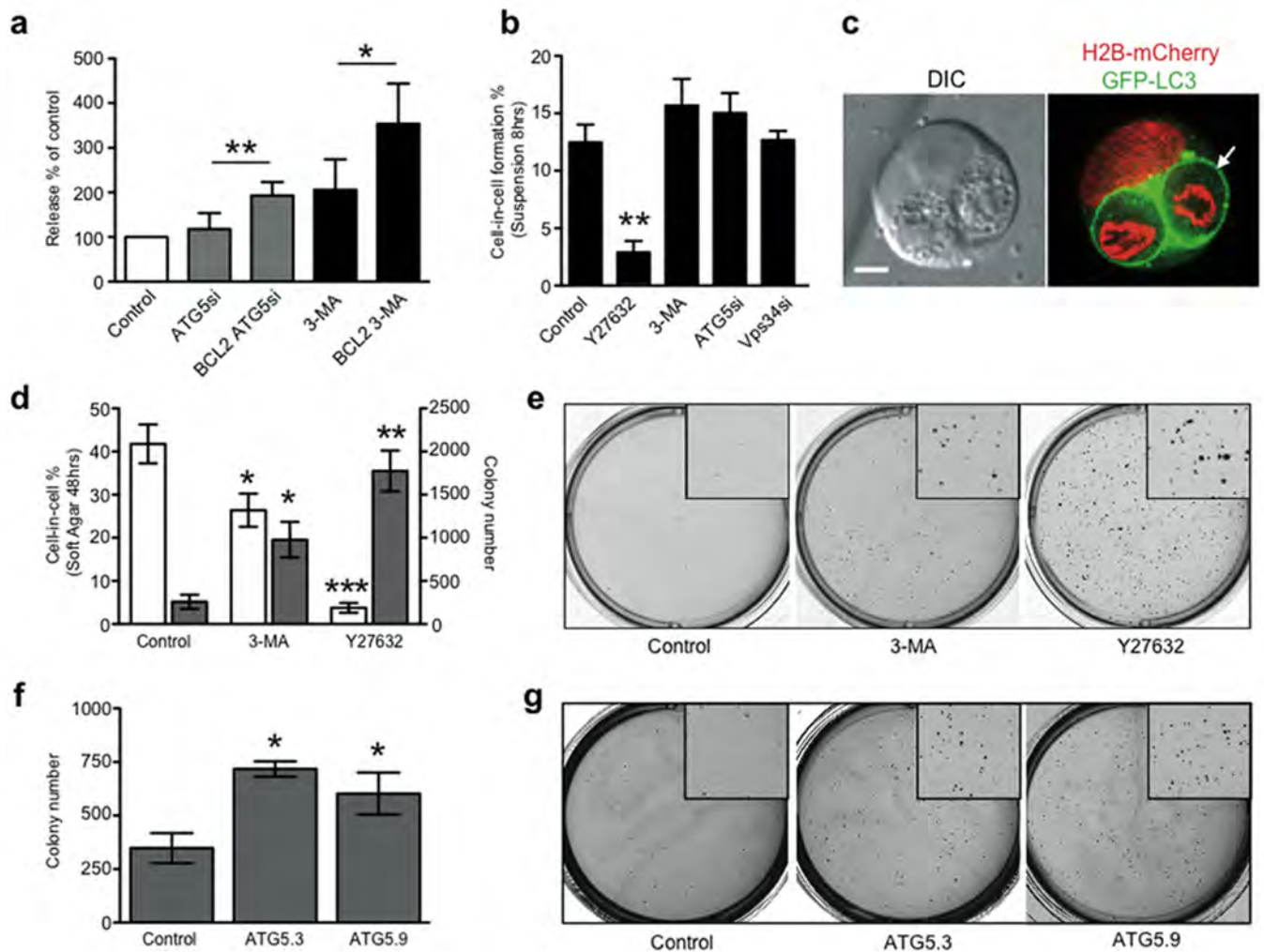
Figure 3.
Inhibition of apoptosis and entotic cell death promotes anchorage-independent growth. (a) The fate of internalized cells (control MCF10A and MCF10A expressing E7 and Bcl2) was measured with and without autophagy inhibition. Data show the percentage of internalized cell release with autophagy inhibition, compared with each control without autophagy inhibition; mean+/− s.e.m. from at least three independent experiments (total cell numbers analysed: ATG5 siRNA, 261 cells; Bcl2 ATG5 siRNA, 97 cells; 3-MA, 170 cells; Bcl2 3-MA, 112 cells); *P < 0:05, **P < 0:02: (b) Effects of Y27632, 3-MA and *VPS34* and *ATG5* siRNA on MCF10A cell-in-cell formation in suspension for 7 hours, >300 cells per condition were scored for cell-in-cell formation, +/− SEM from 3 independent experiments, *P<0.02. (c) Representative image of MCF10A E7+Bcl2 cell-in-cell structure formed in soft agar. Arrow marks LC3 recruitment around internalized cells. Bar = 5µm. (d) Quantification of MCF10A E7+Bcl2 cell-in-cell structures 48 hours after seeding into soft agar (white bars), and colony formation after 2 weeks (gray bars), representative wells are shown in (e). Data represent mean +/− SEM from 3 independent experiments, *P<0.03, **P<0.004, ***P<0.001. (f) Quantification of MCF10A E7+Bcl2 colony formation with Atg5 knockdown with 2 separate siRNAs; representative wells are shown in (g). Data represent mean +/− SEM from 3 independent experiments, *P<0.001. See also Supplementary Information MovieS6.
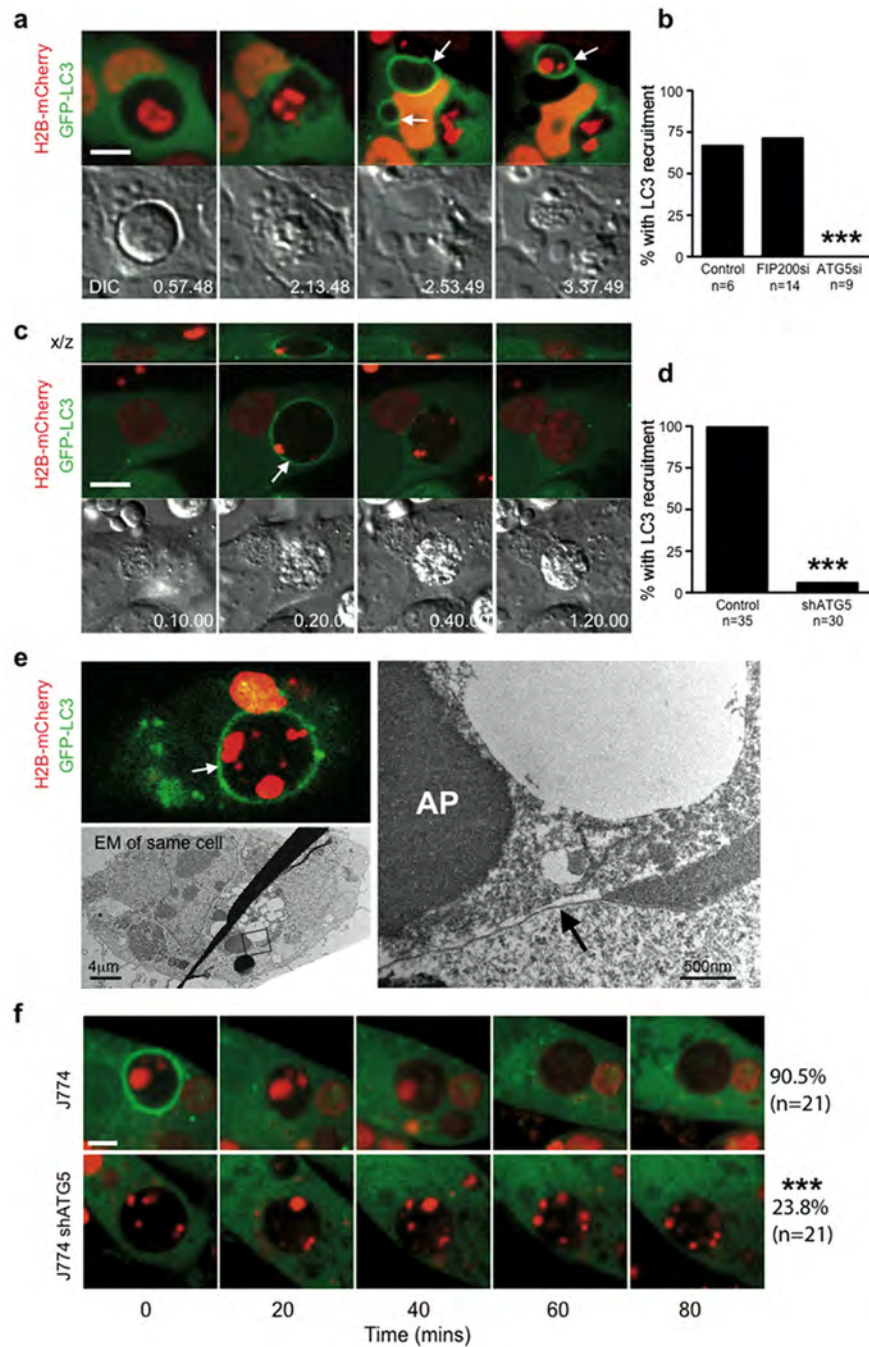
Figure 4.
LC3 recruits to single membrane vacuoles containing apoptotic cells to facilitate corpse degradation. (a) Time-lapse images of MCF10A cell-in-cell structures with internalized cell that undergoes apoptosis. Arrows mark the recruitment of LC3 around apoptotic fragments, see Supplementary Information Movie S7. Bar = 10µm. (b) Quantification of LC3 recruitment to apoptotic internalized cells in the presence of *ATG5* or *FIP200* siRNA (n=number of cells analyzed), ***P<0.0001, chi-square test. (c) Apoptotic U937 cells expressing H2B-mCherry phagocytized by J774 macrophages expressing GFP-LC3. Confocal images show LC3 recruitment to engulfed corpse (arrow), see Supplementary Information Movie S8. Bar = 15µm. (d) Quantification of LC3 recruitment to apoptotic

phagosomes in control and shATG5 expressing cells, ***P<0.0001, chi-square test. (e) Correlative light electron microscopy of an apoptotic phagosome with GFP-LC3 recruitment (top image, white arrow). The LC3-loaded phagosome consists of a single membrane (right image, black arrow) (AP= apoptotic cell nucleus). (f) Representative images of apoptotic cell phagocytosis and degradation in control (n=21) and shATG5 (n=21) J774 GFP-LC3 cells, ***P<0.0001, chi-square test. Bar = 10µm. See also Supplementary Information Fig. S3.
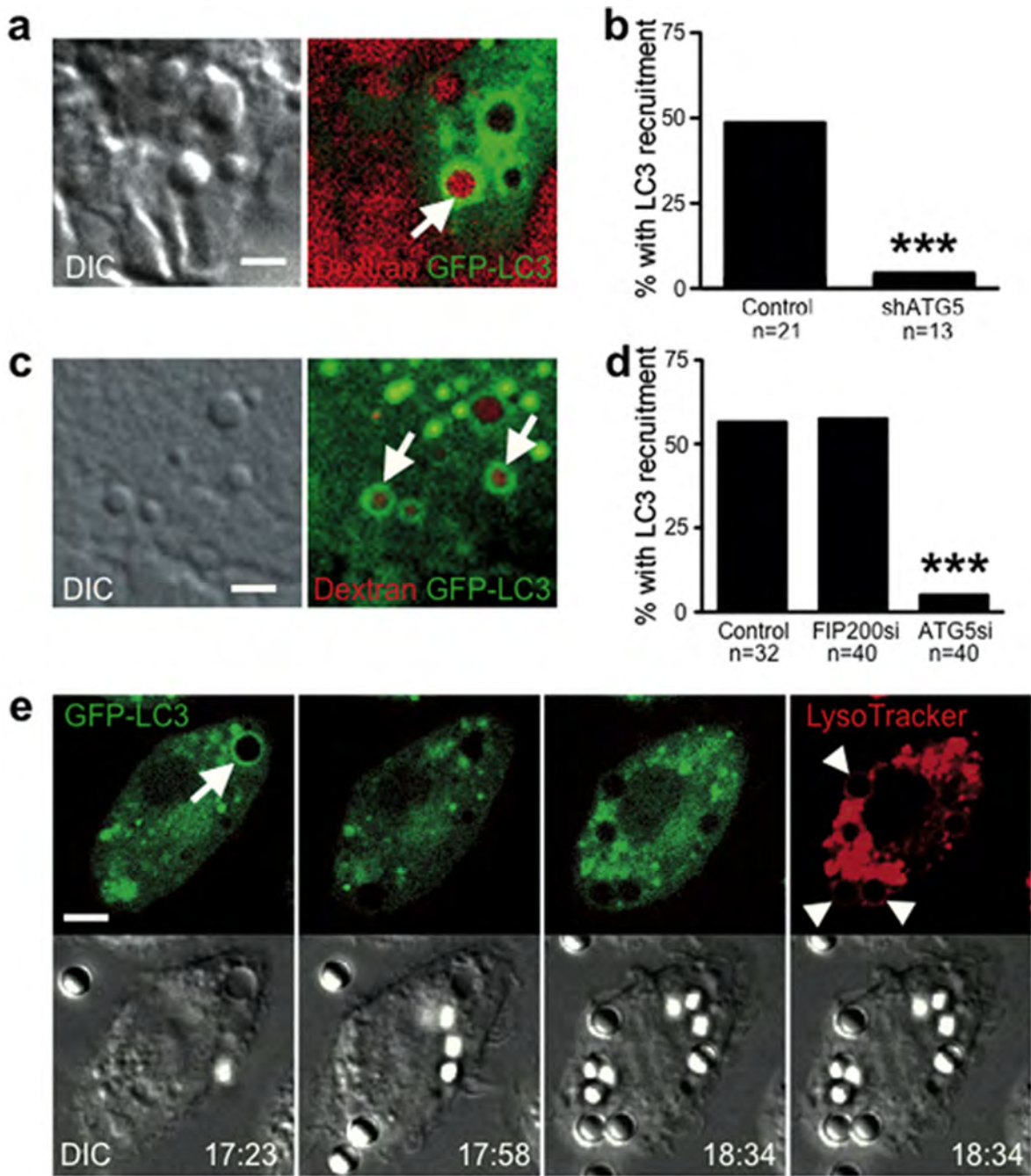
Figure 5.
LC3 recruits to macropinosomes independent of macroautophagy. (a) Representative image of J774 macrophage expressing GFP-LC3 incubated in media containing red dextran. Image shows LC3 recruitment to a dextran-containing macropinosome (arrow). Bar = 2µm. (b) Quantification of LC3 recruitment to macropinosomes in control and shATG5 J774 macrophage; n=number of macropinosomes analyzed, ***P<0.0001, chi-square test. See Supplementary Information Movie S9. c) Representative image of LC3 recruitment to macropinosomes (arrows) in MCF10A cells expressing GFP-LC3 incubated with red dextran. Bar = 2µm. (d) Quantification of LC3 recruitment to macropinosomes in MCF10A cells treated with siRNA against *FIP200* or *ATG5*; n=number of macropinosomes analyzed,

***P<0.0001, chi square test. (e) J774 GFP-LC3 macrophages were incubated with 3µm uncoated latex beads and imaged by confocal microscopy for 1 hour, followed by addition of Lysotracker red to mark acidified compartments. A macropinosome recruited LC3 (arrow) while engulfed latex beads did not (arrow heads). Bar = 5µm. See Supplementary Information Movie S10.
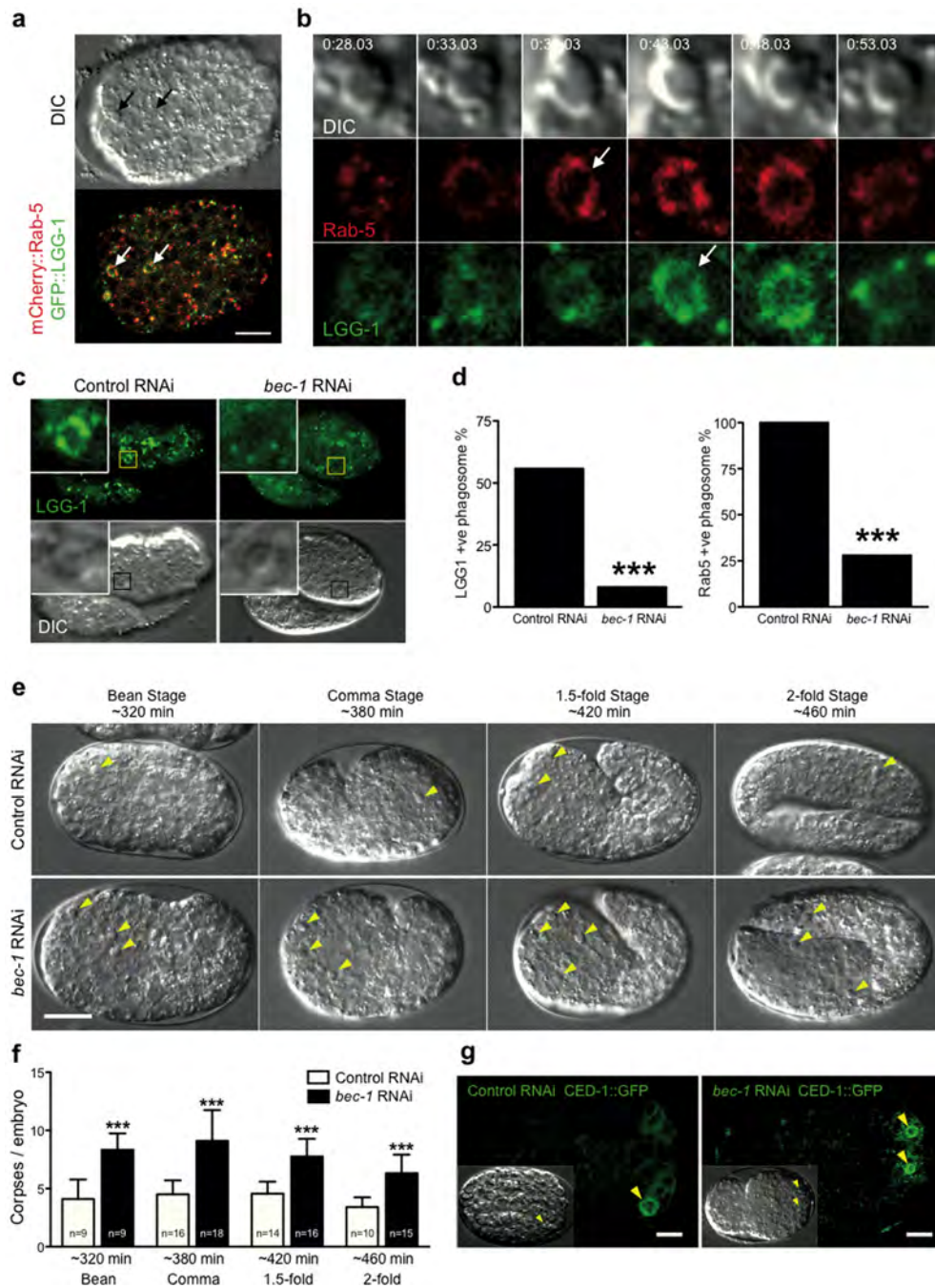
Figure 6.
LGG-1 recruitment to apoptotic phagosomes during *C.elegans* embryonic development. (a) *C. elegans* embryo expressing mCherry::Rab-5 and GFP::LGG-1. Arrows point to two apoptotic phagosomes. See Supplementary Information Movie S11. Bar = 10µm. (b) Cropped time-lapse images showing RAB-5 and LGG-1 recruitment to an apoptotic phagosome (from panel a, left arrow). (c) Representative images of apoptotic phagosomes in embryos from control RNAi or *bec-1* RNAi fed worms. (d) Quantification of GFP::LGG-1 and mCherry::RAB-5 positive phagosomes in control or *bec-1* RNAi embryos determined by time-lapse imaging. Control = 21 embryos, 52 phagosomes, *bec-1* = 9 embryos, 25 phagosomes, ***P<0.0001, chi-square test. (e) Representative DIC images from control and

bec-1 RNAi embryos at different stages of development (minutes post first division). Yellow arrows mark apoptotic corpses. Bar = 10µm. (f) Quantification of apoptotic corpses in control and *bec-1* RNAi embryos, data show +/−SD, P<***0.0001. (g) Representative images of CED-1::GFP embryos with control or *bec-1* RNAi. Yellow arrows mark engulfed corpses surrounded by CED-1::GFP.